Magnetic-field-dependent heat capacity of the single-molecule magnet [Mn(12)O(12)(O(2)CEt) (16)(H(2)O)(3)].

9 AUTHORS, INCLUDING:

Sheila Aubin
Gen-Probe
61 PUBLICATIONS **3,308** CITATIONS

SEE PROFILE

Hilary J Eppley
DePauw University
33 PUBLICATIONS **1,086** CITATIONS

SEE PROFILE

David Hendrickson
University of California, San Diego
599 PUBLICATIONS **26,791** CITATIONS

SEE PROFILE

Michio Sorai
Osaka University
239 PUBLICATIONS **4,232** CITATIONS

SEE PROFILE

Magnetic-Field-Dependent Heat Capacity of the Single-Molecule Magnet [Mn₁₂O₁₂(O₂CEt)₁₆(H₂O)₃]#

Yuji Miyazaki,† **Ashis Bhattacharjee,†,◆** **Motohiro Nakano,‡** **Kazuya Saito,†**
Sheila M. J. Aubin,§ **Hilary J. Eppley,‖,○** **George Christou,‖,▽** **David N. Hendrickson,*,§** and
Michio Sorai*,†,⊥

Research Center for Molecular Thermodynamics, Graduate School of Science, and
Department of Molecular Chemistry, Graduate School of Engineering, Osaka University,
Toyonaka, Osaka 560-0043, Japan, Department of Chemistry and Biochemistry, University of California
at San Diego, La Jolla, California 92093-0358, and Department of Chemistry, Indiana University,
Bloomington, Indiana 47405-4001

Received May 29, 2001

Accurate heat capacities of the single-molecule magnet [Mn₁₂O₁₂(O₂CEt)₁₆(H₂O)₃] were measured from 0.3 to 311 K by adiabatic calorimetry without an external magnetic field. Heat-capacity anomalies were separated by assuming several contributions including lattice vibration, magnetic anisotropy, and hyperfine splitting. Among them, a tiny thermal anomaly between 1 and 2 K is attributable to the presence of Jahn−Teller isomers. The heat capacities of the polycrystalline sample were also measured with applied magnetic fields from 0 to 9 T in the 2−20 K temperature region by the relaxation method. With an applied magnetic field of up to 2 T, a steplike heat-capacity anomaly was observed around the blocking temperature $T_B \approx 3.5$ K. The magnitude of the anomaly reached a maximum at 0.7 T. With a further increase in the magnetic field, the step was decreasing, and finally it disappeared above 3 T. The step at T_B under 0.7 T can be roughly accounted for by assuming that a conversion between the up-spin and down-spin states is allowed above T_B by phonon-assisted quantum tunneling, while it is less effective below T_B. Excess heat capacity under a magnetic field revealed a large heat-capacity hump around 14 K and 2 T, which would be attributed to a thermal excitation from the $S = 9$ ground state to the spin manifold with different S values, where S is the total spin quantum number.

Introduction

Magnetic clusters having a large-spin ground state, such as Mn₁₂ and Fe₈, have currently been attracting many physicists and chemists as a result of their unusual magnetic properties. They are called "single-molecule magnets" because they show hysteresis of magnetization even in a single cluster. They also exhibit characteristics of "superparamagnetism", which is usually encountered in very fine magnetic particles. They give rise to magnetic relaxation because of the interconversion between up- and down-spin states governed by a thermally activated Arrhenius type of relaxation and quantum tunneling of magnetization (QTM).[1−7]

The Mn₁₂ cluster complex [Mn₁₂O₁₂(O₂CMe)₁₆(H₂O)₄]·2MeCO₂H·H₂O (hereafter Mn₁₂Ac), which was first synthesized by Lis in 1980,[8] is a representative single-molecule magnet. The Mn₁₂ cluster comprises an inner cuban cluster containing four Mn(IV) ions (spin quantum number $S = {}^3/_2$), which are interacted ferromagnetically, and an outer ring consisting of eight ferromagnetically interacted Mn(III) ions ($S = 2$). Because the magnetic interaction between the inner cluster and the outer ring is antiferromagnetic, the resultant ferrimagnetic state is stabilized at low temperatures, and the ground spin state becomes $S = 10$.[9] This cluster is characterized by a strong magnetic anisotropy because of the Jahn−Teller distortions arising from the eight Mn(III) ions. Consequently, each Mn-(III) ion exhibits a single-ion zero-field splitting. However, because their distortion axes are oriented parallel to an identical direction (i.e., z axis), one may treat the cluster as if it were a pseudosingle spin. Therefore, the spin Hamiltonial $\hat{H}$ for this system may be written[10−12] as

$$\hat{H} = D\hat{S}_z^2 - g\mu_B\hat{S}B + \hat{H}' \tag{1}$$

where D stands for the uniaxial zero-field splitting parameter for the molecular single spin, g the gyromagnetic ratio, μ_B the Bohr magneton, B the external magnetic field, and $\hat{H}'$ a

(1) DeFranzo, A.; Klik, I.; Gunther, L.; Swanson, A. G.; Brooks, J. S. *J. Appl. Phys.* **1988,** 63, 4234.
(2) Chudnovsky, E. M.; Gunther, L. *Phys. Rev. Lett.* **1988,** 60, 661.
(3) Barbara, B.; Chudnovsky, E. M. *Phys. Lett. A* **1990,** 145, 205.
(4) Awschalom, D. D.; Smyth, J. F.; Grinstein, G.; Divincenzo, D. P.; Loss, D. *Phys. Rev. Lett.* **1992,** 68, 3092.
(5) Awschalom, D. D.; DiVincenzo, D. P.; Smith, J. F. *Science* **1992,** 258, 414.
(6) Gatteschi, D.; Caneschi, A.; Pardi, L.; Sessoli, R. *Science* **1994,** 265, 1054.
(7) Awschalom, D. D.; DiVincenzo, D. P. *Phys. Today* **1995,** 48 (4), 43.
(8) Lis, T. *Acta Crystallogr., Sect. B* **1980,** 36, 2042.
(9) Caneschi, A.; Gatteschi, D.; Sessoli, R. *J. Am. Chem. Soc.* **1991,** 113, 5873.
(10) Politi, P.; Rettori, A.; Hartmann-Boutron, F.; Villain, J. *Phys. Rev. Lett.* **1995,** 75, 537.
(11) Barra, A. L.; Gatteschi, D.; Sessoli, R. *Phys. Rev. B* **1997,** 56, 8192.
(12) Luis, F.; Bartolomé, J.; Fernández, J. F. *Phys. Rev. B* **1998,** 57, 505.

perturbation including hyperfine, quartic, and rhombic zero-field splitting. When $\tilde{H}'$ may be neglected, the spin energy levels are derived as follows:

$$E_{m_s} = D m_s^2 - g \mu_B B m_s \quad (m_s = -S, -S+1, ..., S-1, S)$$

(2)

where m_s is the spin magnetic quantum number. Under a zero magnetic field, the 21-fold degenerated energy levels of the ground $S = 10$ spin state split into 10 doublets and 1 singlet. When D is negative, the $m_s = \pm 10$ levels become the lowest-energy state. This brings about an Ising-type anisotropy. Whenever the magnetic field fulfills the condition of $B = nD/g\mu_B$ (n being an integer), two Zeeman splitting energy levels belonging to different m_s states coincide, and the QTM may occur.[13,14]

Calorimetric[15−23] and magnetic[13,14,17,18,24−29] studies hitherto done for single-molecule magnets fundamentally support the validity of the QTM mechanism. However, such studies have mostly addressed $Mn_{12}Ac$ and $[Fe_8O_2(OH)_{12}(tacn)_6]Br_8 \cdot 9H_2O$ (tacn = triazacyclononane). To throw more light on the magnetic properties of single-molecule magnets, further studies dealing with other single-molecule magnets are desired.

In the present work, we studied an analogous Mn_{12} cluster complex $[Mn_{12}O_{12}(O_2CEt)_{16}(H_2O)_3]$ (abbreviated as $Mn_{12}Pr$), which is obtained by treating $Mn_{12}Ac$ with an excess of $EtCO_2H$ in toluene.[30] X-ray structure analysis[30] of a solvated crystal Mn_{12}-$Pr \cdot 4H_2O$ revealed that this complex crystallizes in the triclinic space group $P\bar{1}$, which has lower symmetry than the tetragonal space group $I\bar{4}$ of $Mn_{12}Ac$.[8] Only three H_2O molecules are ligated to peripheral Mn(III) ions in the present Mn_{12} cluster, different from the coordination of four H_2O molecules in most of the Mn_{12} complexes.[8,28,29,31−33] Magnetization measure-

ments[30] showed that this complex has an $S = 9$ ground state with $D/k_B = -0.86$ K and $g = 1.95$ and that it exhibits a well-defined hysteresis loop. The ac magnetic susceptibility of the powder sample[30] has two peaks in the imaginary component; thus, two different relaxation processes are likely to exist, corresponding to Jahn−Teller isomers.[28,30,32,33]

Heat-capacity calorimetry is one of the powerful experimental methods to elucidate temperature-dependent magnetic behaviors of single-molecule magnets. In this study, we measured heat capacities of $Mn_{12}Pr$ with a magnetic field of up to 9 T to confirm the anomalous spin ground state of $S = 9$ and the presence of Jahn−Teller isomers. We also obtained an interesting temperature and magnetic-field dependence of the heat capacity.

Experimental Section

The present complex was synthesized according to the method reported elsewhere.[30] The elemental analytical result of the desolvated sample is as follows. Anal. Calcd for $Mn_{12}Pr$ ($C_{48}H_{86}O_{47}Mn_{12}$): C, 27.79; H, 4.18; Mn, 31.78. Found: C, 28.15; H, 4.13; Mn, 31.6.

Accurate heat-capacity measurements of the sample without an external magnetic field were performed by the use of two adiabatic calorimeters: a very-low-temperature adiabatic calorimeter workable with a $^3He/^4He$ dilution refrigerator[34] in the 0.3−19 K temperature range and a low-temperature adiabatic calorimeter for small samples in the 7−311 K temperature range.[35] For the former calorimeter, 1.046 60 g of the polycrystalline sample was pressed to form a disk with a 2 cm diameter and loaded into a gold-plated copper cell without any heat exchange medium. For the latter calorimeter, 0.808 65 g of the sample was put into a gold-plated copper cell and sealed with indium wire in 1 atm of a ^4He gas atmosphere to aid thermal equilibration. Buoyancy correction for the sample weights was made by assuming the density of 1.217 g cm^{-3}.[30]

The heat capacities of the complex under a magnetic field were measured with a commercial calorimeter based on the relaxation method (Quantum Design, model PPMS 6000). A small part (1.7461 mg after buoyancy correction) of the disk used for the very-low-temperature heat-capacity measurement was employed for this measurement. It was glued onto the calorimetric platform with a small amount of Apiezon N grease. The heat-capacity measurements were carried out in the temperature region from 2 to 20 K and with applied magnetic fields between 0 and 9 T. The contribution of the addenda (platform + grease) was subtracted from the gross data. The magnetic-field dependencies of the working thermometer (Cernox) and the materials involved in the addenda were examined by measuring the heat capacity of the addenda at various magnetic fields. However, no remarkable difference was detected, even between 0 and 9 T.

Results and Discussion

Heat-capacity results under a zero magnetic field are shown in Figure 1. A very small excess heat capacity between 1 and 2 K and a heat-capacity increase below 0.5 K were observed. Similar thermal anomalies were also found in $Mn_{12}Ac$.[18,23] We shall discuss the origin of these thermal anomalies later.

Heat-capacity data at some magnetic fields are plotted against temperature in Figures 2 and 3. The heat capacity at 0 T increases monotonically with temperature. As the magnetic field is increased, a steplike heat-capacity anomaly appears around

(13) Friedman, J. R.; Sarachik, M. P.; Tejada, J.; Ziolo, R. *Phys. Rev. Lett.* **1996**, *76*, 3830.

(14) Thomas, L.; Lionti, F.; Ballou, R.; Gatteschi, D.; Sessoli, R.; Barbara, B. *Nature* **1996**, *383*, 145.

(15) Novak, M. A.; Sessoli, R.; Caneschi, A.; Gatteschi, D. *J. Magn. Magn. Mater.* **1995**, *146*, 211.

(16) Fominaya, F.; Villain, J.; Gandit, P.; Chaussy, J.; Caneschi, A. *Phys. Rev. Lett.* **1997**, *79*, 1126.

(17) Gomes, A. M.; Novak, M. A.; Sessoli, R.; Caneschi, A.; Gatteschi, D. *Phys. Rev. B* **1998**, *57*, 5021.

(18) Novak, M. A.; Gomes, A. M.; Rapp, R. E. *J. Appl. Phys.* **1998**, *83*, 6943.

(19) Fernández, J. F.; Luis, F.; Bartolomé, J. *Phys. Rev. Lett.* **1998**, *80*, 5659.

(20) Fominaya, F.; Villain, J.; Fournier, T.; Gandit, P.; Chaussy, J.; Fort, A.; Caneschi, A. *Phys. Rev. B* **1999**, *59*, 519.

(21) Sales, M.; Hernandez, J. M.; Tejada, J.; Martínez, J. L. *Phys. Rev. B* **1999**, *60*, 14557.

(22) Fominaya, F.; Gandit, P.; Gaudin, G.; Chaussy, J.; Sessoli, R.; Sangregorio, C. *J. Magn. Magn. Mater.* **1999**, *195*, L253.

(23) Luis, F.; Mettes, F. L.; Tejada, J.; Gatteschi, D.; de Jongh, L. J. *Phys. Rev. Lett.* **2000**, *85*, 4377.

(24) Paulsen, C.; Park, J.-G.; Barbara, B.; Sessoli, R.; Caneschi, A. *J. Magn. Magn. Mater.* **1995**, *140−144*, 379.

(25) Paulsen, C.; Park, J.-G.; Barbara, B.; Sessoli, R.; Caneschi, A. *J. Magn. Magn. Mater.* **1995**, *140−144*, 1891.

(26) Luis, F.; Bartolomé, J.; Fernández, J. F.; Tejada, J.; Hernández, J. M.; Zhang, X. X.; Ziolo, R. *Phys. Rev. B* **1997**, *55*, 11448.

(27) Sangregorio, C.; Ohm, T.; Paulsen, C.; Sessoli, R.; Gatteschi, D. *Phys. Rev. Lett.* **1997**, *78*, 4645.

(28) Aubin, S. M. J.; Sun, Z.; Guzei, I. A.; Rheingold, A. L.; Christou, G.; Hendrickson, D. N. *Chem. Commun.* **1997**, 2239.

(29) Ruiz, D.; Sun, Z.; Albela, B.; Folting, K.; Ribas, J.; Christou, G.; Hendrickson, D. N. *Angew. Chem., Int. Ed.* **1998**, *37*, 300.

(30) Eppley, H. J.; Tsai, H.-L.; de Vries, N.; Folting, K.; Christou, G.; Hendrickson, D. N. *J. Am. Chem. Soc.* **1995**, *117*, 301.

(31) Sessoli, R.; Tsai, H.-L.; Schake, A. R.; Wang, S.; Vincent, J. B.; Folting, K.; Gatteschi, D.; Christou, G.; Hendrickson, D. N. *J. Am. Chem. Soc.* **1993**, *115*, 1804.

(32) Sun, Z.; Ruiz, D.; Rumberger, E.; Incarvito, C. D.; Folting, K.; Rheingold, A. L.; Christou, G.; Hendrickson, D. N. *Inorg. Chem.* **1998**, *37*, 4758.

(33) Sun, Z.; Ruiz, D.; Dilley, N. R.; Soler, M.; Ribas, J.; Folting, K.; Maple, M. B.; Christou, G.; Hendrickson, D. N. *Chem. Commun.* **1999**, 1973.

(34) Murakawa, S.; Wakamatsu, T.; Nakano, M.; Sorai, M.; Suga, H. *J. Chem. Thermodyn.* **1987**, *19*, 1275.

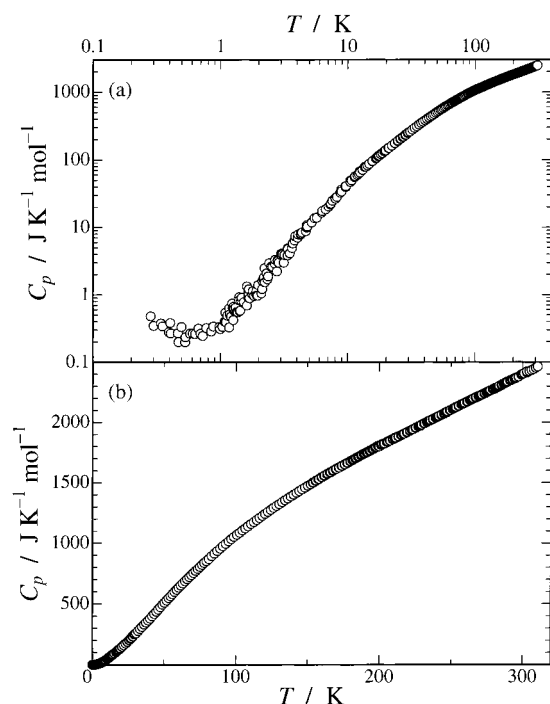(35) Kume, Y.; Miyazaki, Y.; Matsuo, T.; Suga, H. *J. Phys. Chem. Solids* **1992**, *53*, 1297.

Figure 1. Molar heat capacities of $Mn_{12}Pr$ obtained by adiabatic calorimetry on (a) logarithmic and (b) linear scales.
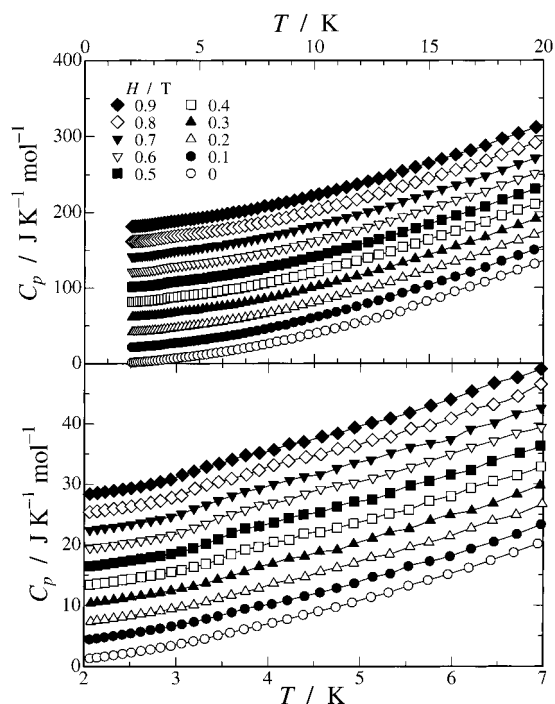

Figure 2. Molar heat capacities of $Mn_{12}Pr$ at lower magnetic fields in (a) whole and (b) low-temperature regions. For the sake of clarity, the origin of each isofield plot is located at intervals of (a) 20 J K^{-1} mol^{-1} and (b) 3 J K^{-1} mol^{-1}.

Figure 3. Molar heat capacities of $Mn_{12}Pr$ at higher magnetic fields in (a) whole and (b) low-temperature regions. For the sake of clarity, the origin of each isofield plot is located at intervals of (a) 20 J K^{-1} mol^{-1} and (b) 3 J K^{-1} mol^{-1}.

Figure 4. Heat-capacity difference between the data obtained under magnetic field $C_p(B)$ and those under a zero field $C_p(0)$ at ($<T_B$, ●) 2.5 K and ($>T_B$, ○) 5 K. The broken curve stands for the simulated Schottky anomaly C_{spin} at 5 K.

3.5 K, corresponding to the blocking temperature. The blocking temperature $T_B \approx 3.5$ K is very close to $T_B \approx 3$ K reported for $Mn_{12}Ac$.[13,25,36] To see a magnetic-field dependence of the heat capacity, we plotted, in Figure 4, the heat-capacity difference between the data obtained under magnetic field B, $C_p(B)$, and those under zero field, $C_p(0)$, at 2.5 K ($<T_B$) and 5 K ($>T_B$). The magnitude of the difference shows a maximum around 0.7
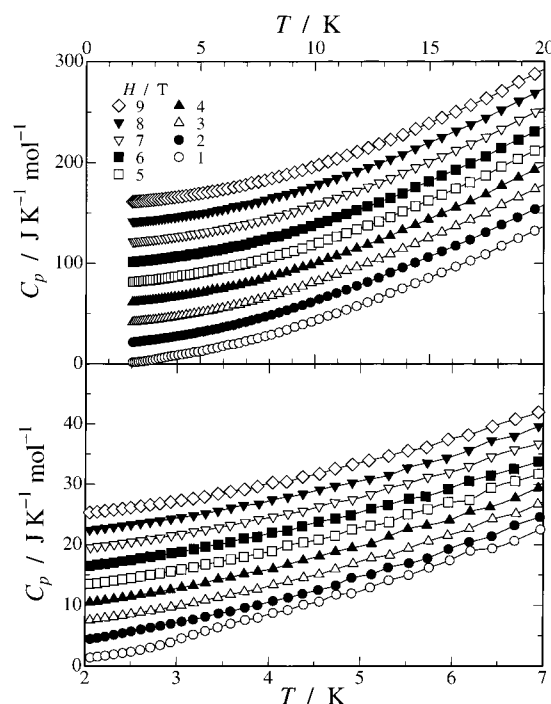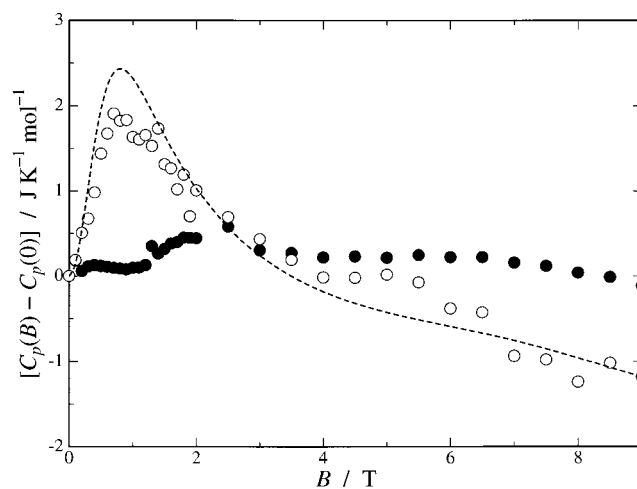
T. As the magnetic field is further increased, the heat-capacity difference, and thus the steplike anomaly, becomes smaller, and it disappears above 3 T. The heat-capacity step at $T_B \approx 3.5$ K is attributable to a glass transition. Below T_B, the conversion between up-spin ($m_s = +S$) and down-spin ($m_s = -S$) states is effectively blocked, and the heat capacity from equilibration between these Zeeman splitting levels $m_s = \pm S$ is diminished. In the case of $Mn_{12}Ac$ single crystals, the thermal anomaly at T_B appeared explicitly at parallel magnetic fields $B = nD/g\mu_B \approx 0.4n$ T, where the spin energy levels make crossing (which is called "phonon-assisted quantum tunneling").[16,20,21] In the case of $Mn_{12}Pr$, we evaluated the level-crossing field to be $B \approx 0.66n$ T, assuming parameters $S = 9$, $D/k_B = -0.86$ K, and $g = 1.95$.[30]

(36) Sessoli, R.; Gatteschi, D.; Caneschi, A.; Novak, M. A. *Nature* **1993**, *365*, 141.
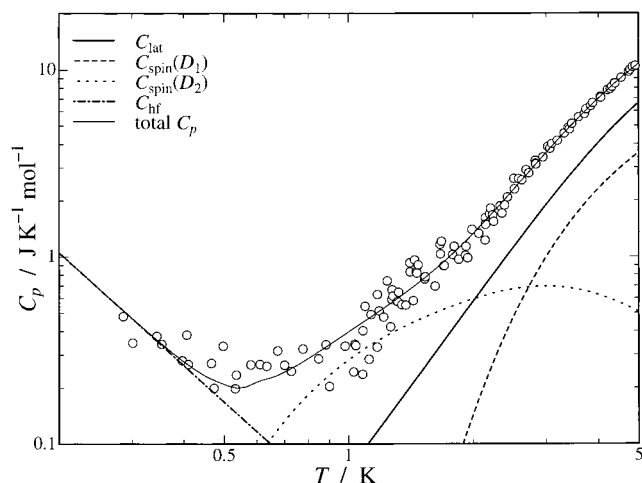
Figure 5. Fitting results of molar heat capacities of $Mn_{12}Pr$ at a zero magnetic field below 5 K. Thick-solid, dashed, dotted, dash−dotted, and thin-solid curves indicate the Debye heat capacity, the spin level heat capacities with D_1 and D_2, the contribution from the hyperfine interaction, and the resultant heat capacity, respectively.

Actually, we observed the largest heat-capacity increase around 0.7 T (see Figure 4).

C_p may involve three different contributions: a lattice vibration (C_{lat}), a Schottky anomaly arising from spin energy levels (C_{spin}), and a hyperfine interaction of Mn nuclei (C_{hf}), that is,

$$C_p = C_{lat} + C_{spin} + C_{hf} \qquad (3)$$

At low temperatures, C_{lat} can be well approximated by the Debye heat capacity with 3 degrees of freedom. The electron-spin heat capacity C_{spin} can be calculated from the energy scheme deduced by eq 1. The heat capacity due to the hyperfine interaction of the Mn nuclei C_{hf} was actually observed in Mn_{12}-Ac.[18,23] In the case of $Mn_{12}Pr$, C_{hf} is remarkably below 0.5 K. In the analysis of the results below 5 K in a zero magnetic field using eq 3, it was revealed that two kinds of spin clusters characterized by different D values should be incorporated into the model. This just corresponds to the Jahn−Teller isomers mentioned previously. A previous magnetic study on $Mn_{12}Pr$[30] also revealed the existence of two different magnetic relaxations, corresponding to two Jahn−Teller isomers. A similar observation was reported by Novak et al.[18] The best-fitting result is as follows: a Debye temperature for 3 degrees of freedom $\Theta_D = 30$ K, two zero-field splitting parameters corresponding to Jahn−Teller isomers, $D_1/k_B = -0.96$ K and $D_2/k_B = -0.19$ K, the fraction of the second component $f_2 = 0.069$, and a contribution from a hyperfine interaction $0.042\ T^{-2}$ J K mol^{-1}. These results are summarized graphically in Figure 5. We performed a similar analysis assuming $S = 10$, but we obtained poorer results. This fact confirms that $Mn_{12}Pr$ has indeed the $S = 9$ ground state.

By applying the optimized parameters ($S = 9$, $g = 1.95$, $D_1/k_B = -0.96$ K, $D_2/k_B = -0.19$ K, and $f_2 = 0.069$) to eq 1 neglecting the perturbation term and also by adopting a powder average concerning the magnetic-field direction, we calculated the $C_{spin}(B) - C_{spin}(0)$ values at 5 K as a function of magnetic field and showed them in Figure 4 by a broken curve. The tendency of the magnetic-field dependence is quite similar between the experimental and calculated values. This fact also supports the validity of the present model.

The estimated Debye temperature $\Theta_D = 30$ K is very close to the values reported previously, $\Theta_D = 36$ K,[15] 38 K,[17] and 41 K[20] for $Mn_{12}Ac$. The D value and the fraction of the minor

species seem to be too small in comparison to those estimated from the ac magnetic susceptibility data.[30] This might arise from a crystal deformation because of a slight difference in the synthesis condition or a slight dehydration from the crystal,[33] which would orient some Mn(III) Jahn−Teller elongated axes to diminish the molecular D value.

Generally, the heat capacity due to a hyperfine interaction appears at very low temperatures, and their high-temperature tails are well approximated by[37]

$$C_{hf} \approx \frac{nN_A k_B}{3}\left(\frac{I+1}{I}\right)\left(\frac{\mu_n \mu_N B_{eff}}{k_B}\right)^2 \frac{1}{T^2} \qquad (4)$$

where n is the total number of nuclei having the nuclear spin quantum number I, N_A Avogadro's number, k_B the Boltzmann constant, μ_n the nuclear magneton number in the unit of a nuclear Bohr magneton (μ_N), and B_{eff} the mean effective magnetic field acting on the nucleus. In the manganese nucleus, $I = {}^5/_2$ for ^{55}Mn and the natural abundance of ^{55}Mn is 100%. Equation 4 can be rewritten by use of the zero-field resonance frequency ν_n of the nucleus as follows:

$$C_{hf} \approx \frac{nN_A k_B}{3}I(I+1)\left(\frac{h\nu_n}{k_B}\right)^2 \frac{1}{T^2} \qquad (5)$$

where h is the Planck constant. By using the resonance frequencies of the ^{55}Mn nucleus (229.8 MHz for four Mn(IV) ions and 285.0 and 365.0 MHz for the respective four Mn(III) ions) observed in nuclear magnetic resonance spectroscopy[38] of $Mn_{12}Ac$ powder crystals at a zero magnetic field, we estimated the hyperfine contribution to be $C_{hf} \approx 0.060\ T^{-2}$ J K mol^{-1}. This estimation is a little bit larger than the experimental value of $0.042\ T^{-2}$ J K mol^{-1}. The slight difference would be attributed to the difference between the resonance frequencies of the ^{55}Mn nucleus in $Mn_{12}Pr$ and in $Mn_{12}Ac$.

The remarkable step behavior around T_B was analyzed by using the parameter set optimized for the zero-field results. As seen from eq 1, above T_B, the C_{spin} term was easily evaluated by a thermal population over $(2S + 1)$-fold spin energy levels under magnetic fields. On the other hand, a trick is required to evaluate nonequilibrium C_{spin} values below T_B. We assumed that the conversion between up-spin and down-spin states is completely forbidden so that it is allowed to make Boltzmann averaging separately for the up-spin and down-spin species, which have their own S-fold energy level schemes. In both cases, above and below T_B, the spin-level schemes were calculated by diagonalizing the spin Hamiltonian (eq 1) without the perturbation term, and the powder-average procedure was adopted for the magnetic-field direction,[39] because the heat-capacity data were obtained for the powder crystalline sample. In Figure 6, $C_p(0\ T)$ and $C_p(0.7\ T)$ are plotted together with the equilibrium C_{spin} (dashed curve) and nonequilibrium C_{spin} (dotted curve). The difference between these two theoretical curves is shown by a thin solid curve. The sum of this difference and $C_p(0\ T)$ is shown in Figure 6 by a thick solid curve for a comparison with $C_p(0.7\ T)$. A small disagreement between $C_p(0.7\ T)$ above T_B and the thick solid curve may be caused by the imperfect powder averaging for the pressed-pellet sample.

(37) Affronte, M.; Lasjaunias, J. C.; Cornia, A.; Caneschi, A. *Phys. Rev. B* **1999**, *60*, 1161.
(38) Goto, T.; Kubo, T.; Koshiba, T.; Fujii, Y.; Oyamada, A.; Arai, J.; Takeda, K.; Awaga, K. *Physica B* **2000**, *284−288*, 1227.
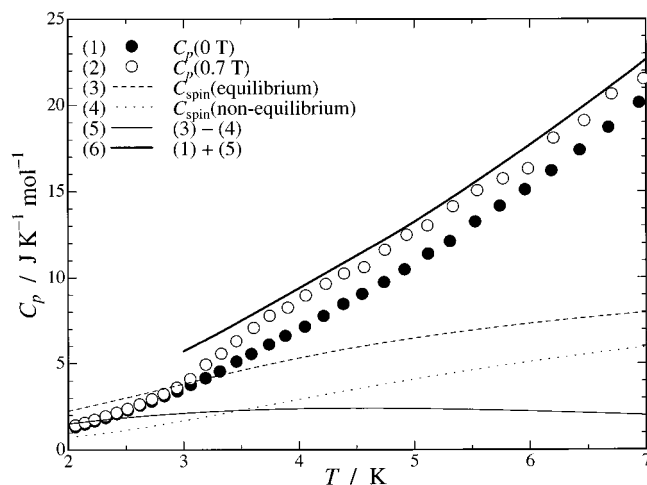(39) Eden, M.; Levitt, M. H. *J. Magn. Reson.* **1998**, *132*, 220.

Figure 6. Molar heat capacities of $Mn_{12}Pr$ at (●) 0 T and (○) 0.7 T. Dotted and dashed curves stand for the Schottky heat capacities calculated from the energy scheme deduced by eq 1 with $B = 0.7$ T when conversion between the up-spin and down-spin states may be forbidden or allowed, respectively. The thin-solid curve implies the difference between these two Schottky heat capacities. The thick-solid curve is the sum of the heat capacity measured at 0 T and the Schottky difference.
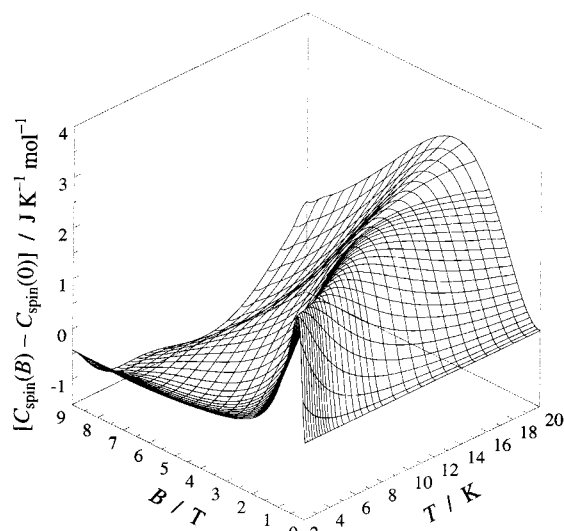

Figure 7. Three-dimensional plot of the difference between the Schottky heat capacities arising from spin energy levels of the $S = 9$ ground state in $Mn_{12}Pr$ with and without magnetic fields against temperature and a magnetic field.

Finally, we shall discuss the temperature and magnetic-field dependence of the heat capacity of $Mn_{12}Pr$ over wide temperature and magnetic-field ranges. Figure 7 shows a three-dimensional plot of the difference between the heat capacities with and without a magnetic field, which are simulated by using the parameters optimized for the zero-field data. The theoretical value below $T_B \approx 3.5$ K is inappropriate, because conversion between up-spin and down-spin states is blocked below T_B. To compare the experimental heat capacities with the theoretical ones, we simultaneously plotted the experimental and theoretical heat-capacity differences at $B = 0.3$, 0.7, 1, 2, and 3 T in Figure 8. As already shown in Figures 2 and 3, a steplike heat-capacity anomaly is found around $T_B \approx 3.5$ K, when the magnetic field is less than 3 T. This anomaly has a maximum at 0.7 T, where the level crossing takes place in the crystallites where the easy axis is aligned parallel to the magnetic field. Interestingly, a large heat-capacity hump was detected around 14 K with a
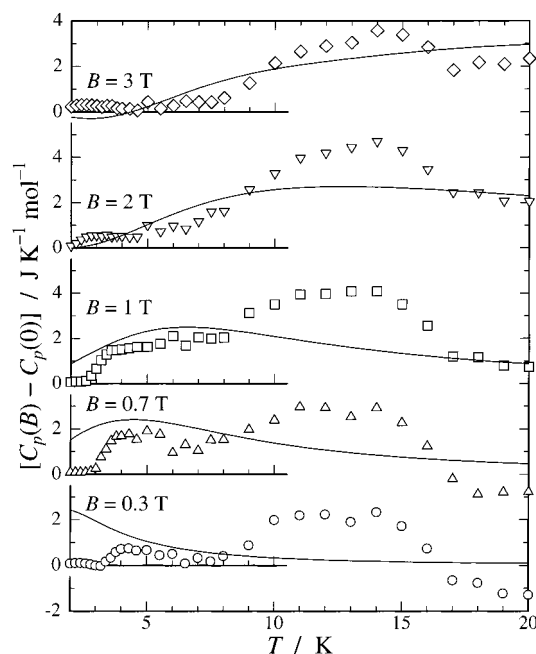

Figure 8. Temperature dependence of the differences between the heat capacities of $Mn_{12}Pr$ with and without a magnetic field at $B = 0.3$, 0.7, 1, 2, and 3 T. The solid curves show the simulated values at the respective magnetic fields.

maximum at 2 T. Because the lattice heat capacity of magnetic materials is scarcely affected by a magnetic field, the present magnetic-field dependence of the heat capacity would be caused by the magnetic-field effect on the spin-level heat capacity C_{spin} deduced from eq 1. The temperature dependence of the experimental heat-capacity difference between 5 and 10 K is similar to that of the theoretical one. This suggests that the heat-capacity difference between 5 and 10 K should arise only from the Schottky contribution of the $S = 9$ ground state. However, the observed thermal anomaly centered around 14 K does not coincide with the theoretical value. This thermal anomaly would be attributed to a thermal excitation from the $S = 9$ ground state to the spin manifold with different S values, presumably $S = 10$ or $S = 8$.

In summary, we measured heat capacities of polycrystalline $Mn_{12}Pr$ not only with a zero magnetic field but also with an applied magnetic field. Analysis of the very-low-temperature heat capacities under a zero magnetic field confirmed the presence of Jahn−Teller isomers. The heat capacities under a magnetic field revealed that a steplike heat-capacity anomaly appears around $T_B \approx 3.5$ K. This steplike anomaly was explained by assuming that the conversion between up-spin and down-spin states is allowed above T_B by phonon-assisted quantum tunneling, while it is not allowed below T_B.

Supporting Information Available: Molar heat capacities of Mn_{12}-Pr by adiabatic calorimetry are provided as Table 1. This material is available free of charge via the Internet at http://pubs.acs.org.